ACS OMEGA

Open Access

http://pubs.acs.org/journal/acsodf

Article

Clickable Probes for Pathogen Proteasomes: Synthesis and Applications

Lawrence J. Liu, Bobby Lucero, Cindy Manriquez-Rodriguez, Karol R. Francisco, Thaiz R. Teixeira, Darius J. Yohannan, Carlo Ballatore, Samuel A. Myers, Anthony J. O'Donoghue,* and Conor R. Caffrey*

Cite This: *ACS Omega* 2024, 9, 34829−34840

Read Online

ACCESS | Metrics & More | Article Recommendations | Supporting Information

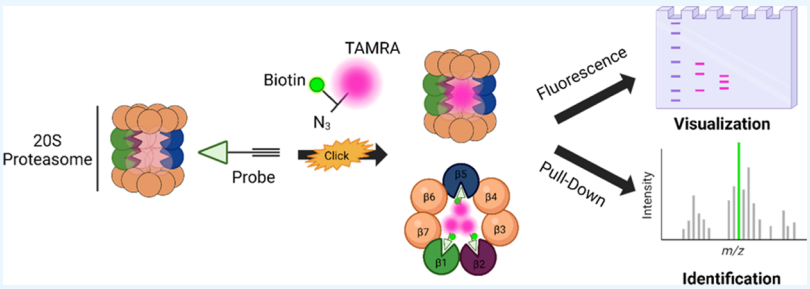

ABSTRACT: The 20S proteasome is a multimeric protease complex that is essential for proteostasis in the cell. Small molecule proteasome inhibitors are approved drugs for various cancers and are advancing clinically as antiparasitics. Although tools and technologies to study the 20S proteasome have advanced, only one probe is commercially available to image proteasome activity. This probe consists of a fluorescently labeled, peptidyl vinyl sulfone that binds to one or more of the catalytic proteasome subunits. Here, we synthesized two, active site-directed epoxyketone probes, LJL-1 and LJL-2, that were based on the peptidyl backbones of the anticancer drugs, carfilzomib and bortezomib, respectively. Each probe was conjugated, via click chemistry, to a bifunctional group comprising 5-carboxytetramethylrhodamine (TAMRA) and biotin to, respectively, visualize and enrich the 20S proteasome from protein extracts of two eukaryotic pathogens, *Leishmania donovani* and *Trichomonas vaginalis*. Depending on species, each probe generated a different subunit-binding profile by sodium dodecyl sulphate-polyacrylamide gel electrophoresis (SDS-PAGE), and the biotin tag enabled the enrichment of the bound subunits which were then formally identified by proteomics. Species differences in the order of electrophoretic migration by the β subunits were also noted. Finally, both probes reacted specifically with the 20S subunits in contrast to the commercial vinyl sulfone probe that cross reacted with cysteine proteases. LJL-1 and LJL-2 should find general utility in the identification and characterization of pathogen proteasomes, and serve as reagents to evaluate the specificity and mechanism of binding of new antiparasitic proteasome inhibitors.

INTRODUCTION

The proteasome is a multisubunit threonine protease that is essential to proteostasis in the cell.[1−3] The 20S catalytic core of the human constitutively expressed proteasome (c20S) is composed of four stacked heptameric rings wherein the outer two rings of α subunits sandwich two β subunit rings, of which, the β1, β2, and β5 subunits are catalytically active[4,5] Each of these active subunits has a preference for cleavage after specific amino acids in a peptide chain, and are categorized as possessing caspase-like (β1), trypsin-like (β2) or chymotrypsin-like activity (β5).[6,7]

Inhibition of the proteasome's catalytic activity is an established therapeutic strategy for various blood cancers, with three inhibitors so far approved.[8−10] In addition, the proteasome is a validated drug target for a number of parasitic diseases,[11−14] and small molecule inhibitors are under development for treatment of malaria[15−18] and in clinical trials for trypanosomatid infections.[19−21]

Over the past decade, the research tools available to characterize the proteasome have advanced on various fronts, and include the use of optimized peptidyl fluorogenic substrates to measure the activity of each of the three catalytic β subunits,[22,23] methodologies to purify the proteasome,[11,24,25] and the availability of cryoEM structures to understand how small molecules engage the target.[16,26,27] Also, active site-directed probes have been developed to define cellular localization, facilitate imaging in small animal models and understand the specificities of small molecule proteasome inhibitors.[28−30]

Received: May 6, 2024
Revised: July 25, 2024
Accepted: July 26, 2024
Published: August 2, 2024

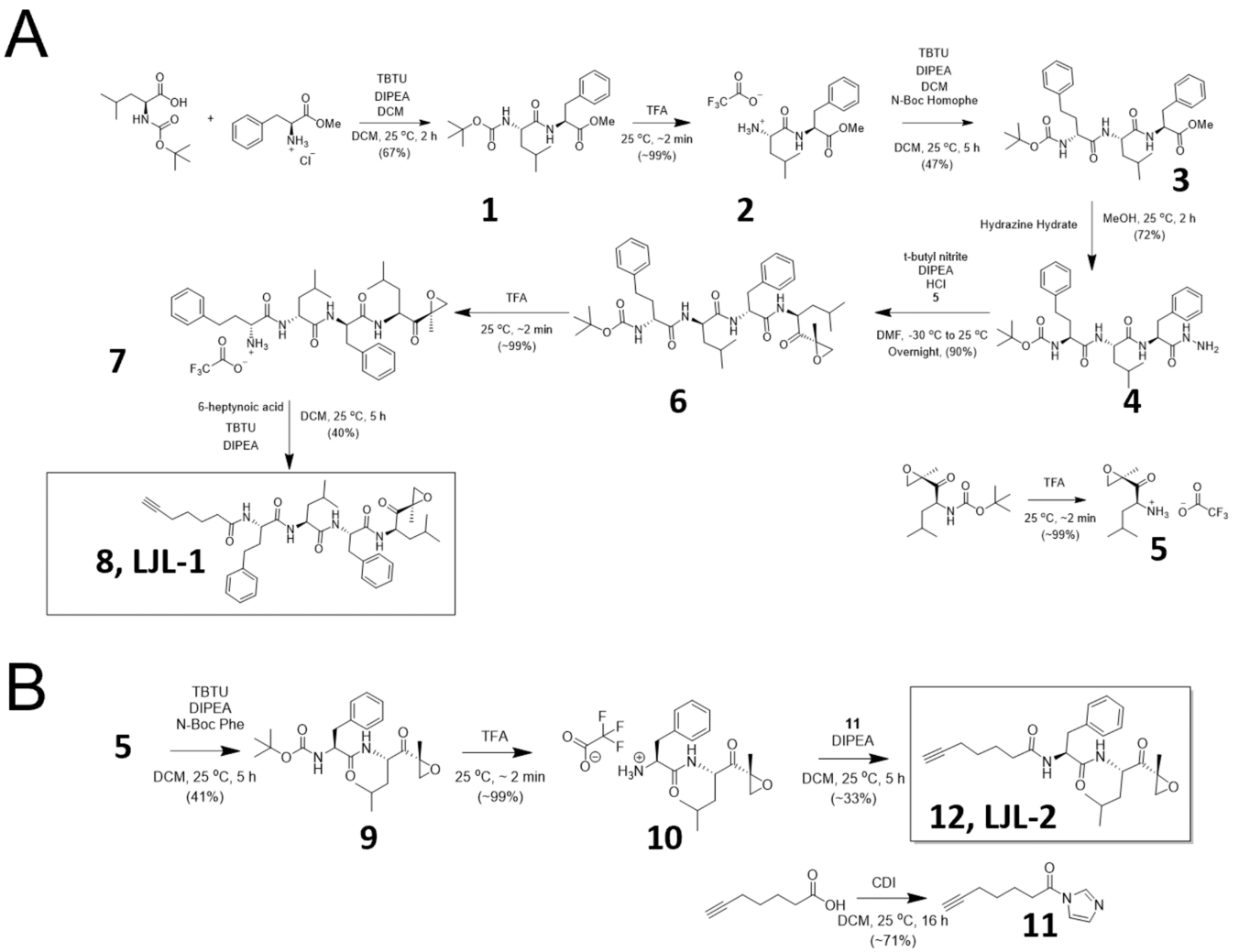

Figure 1. Synthetic schemes for LJL-1 (A) and LJL-2 (B).

In terms of active site-directed probes with which to visualize c20S (*e.g.*, after native or denaturing gel electrophoresis), the most commonly used is the irreversible, fluorescent, peptidyl vinyl sulfone, Me_4BodipyFL-Ahx$_3$L$_3$VS (Figure 2A), a derivative of the originally described MV151 (Bodipy TMR-Ahx$_3$L$_3$VS).[29,31] During our efforts to characterize parasite 20S molecules as potential drug targets, we identified limitations to this probe. Specifically, it binds irreversibly to cysteine proteases (SI 1), which are often highly expressed in parasites,[32,33] and sometimes labels just two of the three catalytic β subunits[22,23] even though the genomic/proteomic evidence indicates the presence of all three. Lastly, Me_4BodipyFL-Ahx$_3$L$_3$VS lacks the functionality to enable isolation of the catalytic β subunits from protein extracts which would then facilitate their identification via proteomics. Combined, these limitations complicate the biochemical analysis of parasite proteasomes, information that is necessary for a campaign to develop specific antiparasitic proteasome inhibitors.

Given the above limitations, we synthesized two activity-based probes that are based on the peptidyl scaffolds of the proteasome inhibitor drugs, carfilzomib (CFZ) and bortezomib (BTZ). These probes were designed with an N-terminal alkyne group to allow the attachment of an azide-containing reagent via click chemistry, in this case, a bifunctional group consisting of 5-carboxytetramethylrhodamine (TAMRA) and biotin. For two parasite species, we describe the utility of each probe to engage and visualize the 20S proteasome in cell extracts as well as enrich the target for identification of the constituent catalytic β subunits.

RESULTS

We used the peptidyl backbones of the proteasome inhibitors, CFZ and BTZ, to synthesize two epoxyketone-based 20S probes. After binding of the probes to the target proteasome, they were then conjugated to a bifunctional group comprising TAMRA and biotin via bioorthogonal copper(I)-catalyzed azide−alkyne cycloaddition (CuAAC).[34] These probes facilitated the visualization and identification of the catalytic β subunits of the target proteasome in parasite extracts.

Synthesis of LJL-1 and -2, and Their Differential Engagement of c20S Subunits. Alkyne-homoPhe-Leu-Phe-Leu-epoxyketone (**8**, LJL-1; Figure 1A) is an analog of CFZ, an FDA-approved proteasome inhibitor. The alkyne group on LJL-1 allows coupling to TAMRA-Biotin azide via standard click chemistry.

The synthesis of LJL-1 was accomplished by first coupling the amino acids at P2−P4, Phe-Leu-homoPhe, using TBTU-based peptide synthesis to generate **3**. This was followed by a conversion of the methyl ester into a hydrazide (**4**) and then

https://doi.org/10.1021/acsomega.4c04316
ACS Omega 2024, 9, 34829−34840

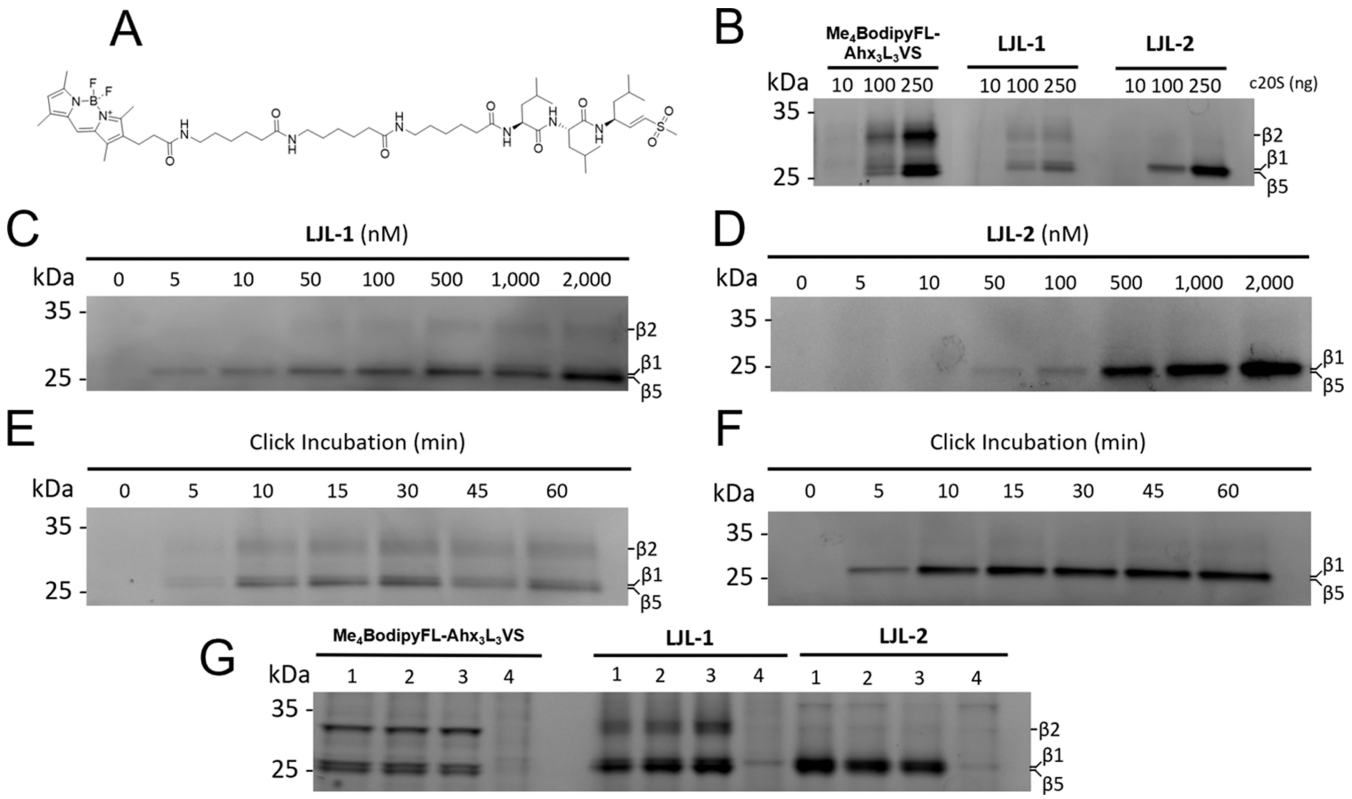

Figure 2. Probe engagement with purified c20S and HepG2 cell lysate under various conditions. (A) Structure of Me_4BodipyFL-Ahx_3L_3VS. (B) Florescence imaging of c20S β subunit banding patterns labeled by Me_4BodipyFL-Ahx_3L_3VS, LJL-1 and LJL-2. (C, D) Concentration-dependent binding of LJL-1 and LJL-2, respectively, to 100 ng c20S. (E, F) Time-dependence of the click reaction for LJL-1 and LJL-2, respectively, with 100 ng c20S. (G) Subunit banding patterns generated by Me_4BodipyFL-Ahx_3L_3VS, LJL-1, and LJL-2 with 16 μg HepG2 cell lysate. Lysate was preincubated with (1) DMSO, (2) 20 μM E64, (3) 2 mM PMSF or (4) 10 μM MZB, prior to addition of probe.

oxidation to an acyl azide that allowed peptide coupling to the leucine epoxyketone fragment (**5**) which yielded the tetrapeptide-epoxyketone, **6**. The Boc-protected precursor of **5** was purchased. Finally, deprotection of the N-Boc-protected homophenylalanine (**7**) allowed the alkyne to be attached using TBTU chemistry to yield **8**, which was named LJL-1 (Figure 1A).

The peptidyl sequence for the second probe, alkyne-Phe-Leu-epoxyketone (**12**, LJL-2; Figure 1B) was based on the FDA-approved proteasome inhibitor, BTZ. We replaced the reversible and covalent boronate warhead of BTZ[9] with an irreversibly-binding epoxyketone.[35]

The synthesis of LJL-2 was accomplished via TBTU-based peptide coupling between the leucine epoxyketone fragment, **5**, and an N-Boc-protected phenylalanine, followed by Boc-deprotection and subsequent *N*-acylation reaction with the acyl imidazole, **11** (Figure 1B).

The evaluation of Me_4BodipyFL-Ahx_3L_3VS (Figure 2A) alongside LJL-1 and LJL-2 using pure c20S revealed distinct binding patterns after sodium dodecyl sulphate-polyacrylamide gel electrophoresis (SDS-PAGE) and fluorescent imaging. The slight misalignment of the c20S β subunit banding patterns can be attributed to the different molecular masses of each probe: Me_4BodipyFL-Ahx_3L_3VS (1059.2 amu), LJL-1 (1875.3 amu), and LJL-2 (1600.9 amu). As anticipated, Me_4BodipyFL-Ahx_3L_3VS binds to all three catalytic β subunits (Figure 2B).[29,36] Similarly, LJL-1 binds all three subunits with a stronger preference for β5 and β1 relative to β2. In contrast, LJL-2 binds strongly to the lower subunits, which seem to be composed of β1 and β5. Titrating LJL-1 with pure c20S shows preferential binding to the β5 subunit, with both β1 and β2 being labeled only at higher concentrations (Figure 2C). Titrating LJL-2 demonstrates labeling of β1 and β5 (Figure 2D), but with a weaker limit of detection of c20S compared to LJL-1, *i.e.*, 50 *vs.* 5 nM. Lastly, the time needed for the click reaction between the azide and alkyne to proceed to completion was ~10 min for both probes (Figure 2E,F).

To verify probe selectivity for c20S in cell extracts, we preincubated HepG2 cell lysates with three class-specific protease inhibitors, namely, E64 (cysteine proteases), phenylmethylsulfonyl fluoride (PMSF; serine proteases) and marizomib (MZB; proteasome) prior to addition of probe (Figure 2G). The binding patterns resolved for the DMSO controls were essentially identical to those noted for pure c20S (Figure 2B), *i.e.*, three subunits using Me_4BodipyFL-Ahx_3L_3VS and LJL-1, and two subunits (appearing as one fused band) with LJL-2. Of the inhibitors tested, only MZB abolished binding by all three probes, confirming the identities of the bands as c20S catalytic β subunits. When evaluated for inhibition of growth of HEK293 cells *in vitro*, LJL-1 and LJL-2 generated similar EC_{50} values to those of CFZ and BTZ with values in the range of 5−20 nM (SI 2). Thus, the substitution of the N-terminal morpholine cap in CFZ for the alkyne group in LJL-1, and the substitution of the N-terminal pyrazine and the C-terminal boronate warhead in BTZ for the alkyne and epoxyketone, respectively, in LJL-2, did not dramatically alter compound potency.

We next tested the ability of LJL-1 and LJL-2 to inhibit the individual β subunits of c20S in a microplate assay using β subunit-specific substrates as reporters of enzyme activity

https://doi.org/10.1021/acsomega.4c04316
ACS Omega 2024, 9, 34829−34840

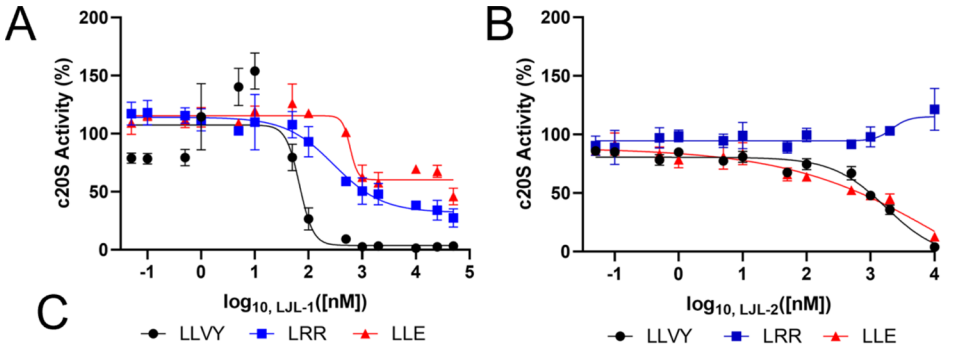

Inhibitor	β1 IC_{50} (nM)	β2 IC_{50} (nM)	β5 IC_{50} (nM)
LJL-1	> 50,000	596 ± 27	68 ± 32
Carfilzomib	> 50,000	43,359 ± 5184	153 ± 52
LJL-2	2157 ± 27	> 50,000	1725 ± 42
Bortezomib	65 ± 55	> 50,000	97 ± 41

Figure 3. Inhibition of c20S catalytic β subunits by LJL-1 and LJL-2. Concentration-dependent inhibition by (A) LJL-1 and (B) LJL-2 of each the c20S β subunits (100 ng enzyme) using subunit-specific peptidyl AMC substrates, *i.e.*, LLVY (β5), LRR (β2) and LLE (β1). C. EC_{50} values for the various proteasome inhibitors. Assays with LJL-1 and LJL-2 were performed twice each in triplicate (n = 6). Assays with CFZ and BTZ were performed once in triplicate (n = 3).

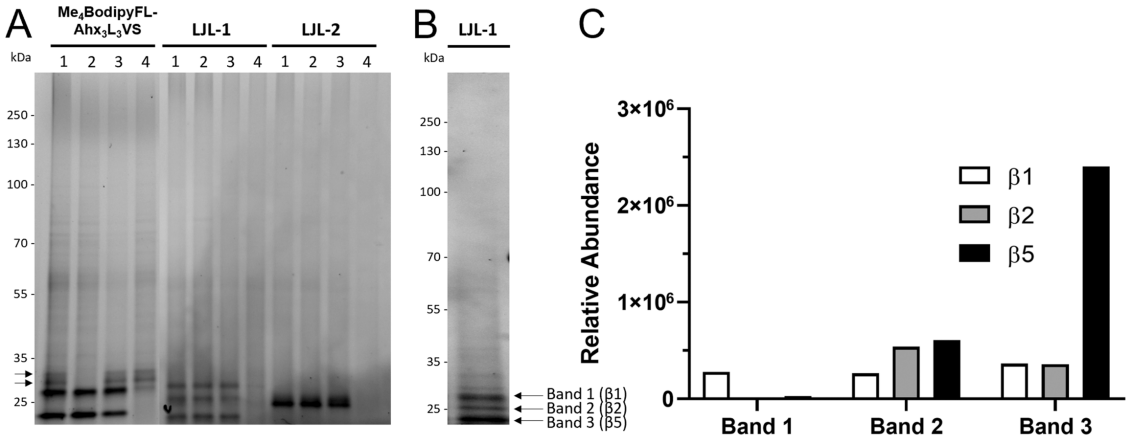

Figure 4. Probe engagement with, and enrichment and identification of *L. donovani* promastigote catalytic β subunits. (A) Fluorescence imaging of banding patterns generated by Me_4BodipyFL-Ahx_3L_3VS, LJL-1 and LJL-2 in cell lysate. Lysate (16 μg) was preincubated with (1) DMSO, (2) 20 μM E64, (3) 2 mM PMSF or (4) 10 μM MZB prior to addition of probe. Engagement of cysteine proteases (bands sensitive to E64) by Me_4BodipyFL-Ahx_3L_3VS is marked with black arrows. (B) Fluorescence imaging of 20S β subunits (three bands) after enrichment from parasite lysate using the biotin functionality of LJL-1. (C) Label-free peptide quantification of each of the excised subunit bands.

(Figure 3 and SI 3).[37−39] LJL-1 was 2- and 73-fold more potent than CFZ at targeting the β5 and β2 subunits, respectively, and neither compound inhibited the β1 subunit (Figure 3A,C). LJL-2 inhibited only β1 and β5, and for each respective subunit, was 33- and 18-fold weaker than BTZ (Figure 3B,C). Neither LJL-2 nor BTZ engaged the β2 subunit, even at the highest concentration of 50 μM tested. The decreased binding capacity of LJL-2 compared to BTZ suggests that the boronate warhead in BTZ confers stronger proteasome engagement. Although this enhanced interaction might be favorable for therapeutic applications, boronates cross react with serine proteases, thus compromising probe selectivity.[40]

Overall, we show that both LJL probes can directly and indirectly characterize the catalytic β subunits of a target proteasome. Directly, the probes can be labeled with a fluorogenic reporter molecule after they have bound to the target subunit and the banding pattern then visualized via SDS-PAGE (Figure 2B,G). Indirectly, the probes can be employed as inhibitors that compete with the fluorogenic reporter substrates for binding to the catalytic β subunits (Figure 3).

Parasite Proteasome Engagement and β Subunit Identification Using LJL-1 and -2. Understanding the connection between inhibition of one or more 20S β subunit and antiparasitic activity is fundamental to designing parasite-specific proteasome inhibitors. Employing a similar experimental design to that shown in Figure 2G with extracts of *Leishmania donovani* promastigotes and class-specific protease inhibitors (Figure 4A), we found that the commercial probe, Me_4BodipyFL-Ahx_3L_3VS, labeled just two of the three 20S β subunits, in addition to cysteine proteases which are abundant in this parasite.[32,41] Engagement of cysteine proteases by Me_4BodipyFL-Ahx_3L_3VS is not surprising given that vinyl sulfone warheads react with the cysteine nucleophile in such

https://doi.org/10.1021/acsomega.4c04316
ACS Omega 2024, 9, 34829−34840

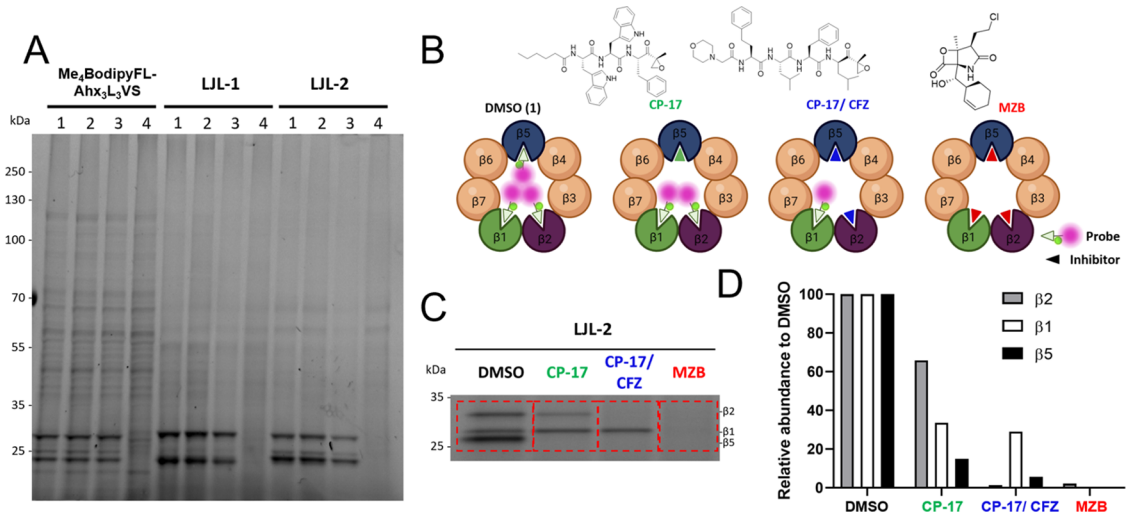

Figure 5. Probe engagement with, and enrichment and identification of, *T. vaginalis* catalytic β subunits. (A) Fluorescence imaging of banding patterns generated by Me_4BodipyFL-Ahx_3L_3VS, LJL-1 and LJL-2 in parasite cell lysate. Lysate (16 μg) was preincubated with (1) DMSO, (2) 20 μM E64, (3) 2 mM PMSF or (4) 10 μM MZB, prior to addition of probe. (B) Schematic of inhibitor or inhibitor combinations known to inhibit one or more Tv20S β subunits.[23] (C) Fluorescence imaging of Tv20S β subunits after incubation with β subunit-specific inhibitors or combinations of inhibitors, and enrichment from parasite lysate using the biotin functionality of LJL-2. (D) Label-free peptide quantification in each of the excised gel pieces (red boxes in (C)) that identifies each of the β subunits as a function of the inhibitor or combinations of inhibitors employed.

proteases.[42−44] By contrast, LJL-1 labeled three protein species, and this binding could be blocked by prior incubation with the broad-spectrum proteasome inhibitor, MZB. LJL-2 labeled a single subunit that was also inhibited by MZB (Figure 4A). Thus, and as seen with the HepG2 lysate, each probe resolves a different catalytic β subunit pattern.

Because LJL-1 labeled all three catalytic β subunits in the *L. donovani* lysate, we employed the biotin functionality to enrich the proteasome from lysate using neutravidin-bead chromatography. After binding, the beads were extensively washed, then boiled to release the biotin-bound proteins, and the supernatant was resolved by SDS-PAGE (Figure 4B). With the aid of the TAMRA functionality, each of the three subunits was visualized, excised and identified by proteomics as β1 (Uniprot ID: A0A504 × 6A3), β2 (A0A3S7XA80), and β5 (A0A3Q8IIY4), from highest to lowest molecular weight (Figure 4C). Thus, the combined functionalities of the biotin and TAMRA components bound to LJL-1 were critical to identifying the three catalytic β subunits in*L. donovani* promastigotes and, further, demonstrated that their order of electrophoretic migration (β1, β2 and β5; highest to lowest) differs from that for HepG2 cells (β2, β1 and β5).

Using a second parasite,*Trichomonas vaginalis*, each of the three probes again showed differential binding to either two or three protein species in cell lysate that could be inhibited by prior incubation with MZB (Figure 5A). Notably, the background was less pronounced with LJL-1 and LJL-2 compared to that with Me_4BodipyFL-Ahx_3L_3VS. Previous research using purified Tv20S identified the electrophoretic migration order of the β subunits as β2, β1, and β5, from highest to lowest molecular weight.[23] Accordingly, we wished to employ inhibitors that selectively inactivate one or other β subunit such that the uninhibited subunit(s) would be available to bind to the probe. These subunits could then be isolated and visualized. In this case, LJL-2 was chosen as it bound to all three β subunits.

A number of 20S inhibitors and inhibitor combinations have been shown to preferentially inhibit one or more Tv20S catalytic β subunits.[23] The carmaphycin B analog, CP-17[45] selectively inhibits β5 at 1 μM. CP-17 and CFZ at 10 μM inhibit both β5 and β2, and MZB at 10 μM inhibits all three subunits (Figure 5B). These inhibitors were incubated with*T. vaginalis* lysate prior to addition of LJL-2, which then bound to the uninhibited β subunits for their eventual visualization by SDS-PAGE after biotin-neutravidin chromatography (Figure 5C). For proteomic analysis, a large gel slice was excised from each lane, which corresponded to the region in which the three catalytic subunits had migrated (Figure 5C, red boxes). The excision step was much easier to perform than the precision required with the *L. donovani* samples above. Subsequent proteomic analysis demonstrated the utility of the strategy whereby the DMSO control lane had the highest relative abundance of each of the three β subunits (Figure 5D). Following pretreatment with CP17, β5 subunit abundance was decreased by 6.7-fold whereas those for β1 and β2 subunits were only reduced by 1.5- and 3-fold, respectively. This indicates that CP-17 preferentially targets the β5 subunit (the lowest subunit on the gel; Figure 5C). Treatment with a combination of CP-17 and CFZ did not change the abundance of the β1 protein whereas those for the other two subunits were decreased. Accordingly, the remaining subunit visible in the CP-17/CFZ lane on the gel is the β1 subunit. MZB inhibited all three subunits (Figure 5C) with the consequence of little to no binding signal being returned by the probe (Figure 5D). Overall, the approach outlined here offers an alternative method to identifying individual catalytic β subunits in parasite lysates that circumvents the need to carefully excise individual and closely juxtaposed subunits from a gel.

DISCUSSION

The proteasome is an attractive antiparasitic drug target,[14,46,47] and small molecule inhibitors are preclinically progressing for treatment of malaria[15−18] or in the clinic for trypanosomatid diseases.[19−21] As described above, the tools to visualize and characterize the proteasome have advanced, however, just one activity-based probe, Me_4BodipyFL-Ahx_3L_3VS,[29] is commer-

https://doi.org/10.1021/acsomega.4c04316
ACS Omega 2024, 9, 34829−34840

cially available. As shown here for parasitic organisms, this probe is not selective for the 20S proteasome as it reacts with cysteine proteases[44] which are abundant in many parasites,[32,33] including *L. donovani*.[41] Further, unlike the situation for human c20S in HepG2 cell extracts, the commercial probe does not consistently label all three catalytic β subunits in parasite extracts, with two subunits being labeled in *L. donovani* promastigotes and three in *T. vaginalis*. Last, the commercial probe was not designed to allow the identification of the individually resolved subunits.

Accordingly, to advance research into parasite 20S proteasomes as drug targets, we employed bioorthogonal copper(I)-catalyzed azide−alkyne cycloaddition (CuAAC),[34] or "click chemistry" to synthesize *bifunctional* probes to enable the isolation of the 20S from cell extracts and the identification of the component catalytic β subunits. LJL-1 and LJL-2 were based on the peptidyl backbones of the anticancer drugs, CFZ and BTZ, respectively, which have well understood c20S β subunit binding preferences,[48] and so far, seem to be universally antiparasitic via engagement of the 20S proteasome.[11−14] Using two example parasites, *L. donovani* and *T. vaginalis*, the bifunctional probe strategy to isolate and identify 20S catalytic β subunits without interference by cysteine proteases worked well and should be more straightforward to implement than alternative, time-consuming multistep 20S purification methods,[22,23] and the requisite for large quantities of often limiting and expensive parasite material. The probes also demonstrated that the order of electrophoretic migration of the β subunits is parasite-dependent and may not align with the profile established for human cells, similar to a previous finding for *Plasmodium falciparum* 20S using a fluorescent epoxyketone probe, BMV037.[15,16] Lastly, the single, dual functionality probe containing both a fluorophore and biotin tag, is efficient compared to the time and costs associated with the need to synthesize separate probes for each functionality, *e.g.*, the serine hydrolase probes, biotin-fluorophosphonate and TAMRA- fluorophosphonate.[49,50]

The downstream utility of probes containing reactive alkynes is broad and a variety of azide-containing reagents can be coupled after labeling of the catalytic 20S β subunit(s).[51,52] In addition, rather than alkyne-containing APBs, the next generation probes could substitute the alkyne for difluorinated cyclooctyne[53] or bicyclo[6.1.0]nonyne,[54] which would allow for real-time *in vivo* fluorescence imaging of proteasome activity, and its inhibition, using copper-free click chemistry. Also, biotin, as a purification handle, may be substituted by desthiobiotin, which has a lower binding affinity,[55] or by cleavable biotin linkers,[56] which would aid in the release of bound proteins after affinity purification. Finally, click chemistry could be used to conjugate a parasite-specific antibody to a proteasome inhibitor,[57] potentially improving on-target potency while minimizing host toxicity.

The importance of developing two probes based on tetrapeptidyl and dipeptidyl backbones is highlighted by the different SDS-PAGE profiles resolved for the 20S catalytic β subunits in HepG2 cells, *L. donovani* and*T. vaginalis*. Had we relied on just one or other probe, we would likely have been unable to enrich for and identify all three β subunits depending on the parasite. This realization comes after the fact and is fortuitous as we had originally intended to synthesize just LJL-1, and it may yet be the case that additional activity-based probes will be needed to functionally investigate other pathogen 20S proteasomes, including with respect to the development of potent and selective antiparasitic proteasome inhibitors.

CONCLUSIONS

Two activity-based, epoxyketone probes, LJL-1 and LJL-2, were synthesized and each conjugated, via click chemistry, to a bifunctional TAMRA and biotin handle. The probes were then used to enrich the 20S proteasome from lysates of HepG2 cells, *L. donovani* promastigotes or*T. vaginalis*, and enable the identification of the respective catalytic β subunits. Compared to a commercially available vinyl sulfone probe, the new probes did not cross-react with cysteine proteases and revealed that the order of β subunit electrophoretic migration can differ depending on the originating species. As interest in the 20S proteasome as a drug target for treatment of parasitic infections expands, both probes will aid the characterization of the 20S in complex cell extracts and support efforts to improve the potency and specificity of antiparasitic 20S β subunit inhibitors.

METHODS

All solvents were of reagent grade. All reagents were purchased from Alfa Aesar or Fisher and used as received. Thin-layer chromatography (TLC) was performed with 0.25 mm E. Merck precoated silica gel plates. Silica gel column chromatography was performed with silica gel 60 (pore volume 0.74−0.84 mL/g) supplied by Millipore Sigma (#105554). TLC spots were detected by viewing under a ultraviolet (UV) light. Proton (^{1}H) was recorded on a 500 MHz Bruker AMX-500 spectrometer and on a 600 MHz Bruker AVANCE III spectrometer. Chemical shifts were reported relative to solvents. Data for ^{1}H NMR spectra are reported as follows: chemical shift [ppm, referenced to protium; s = singlet, d = doublet, t = triplet, q = quartet, quint = quintet, dd = doublet of doublets, td = triplet of doublets, ddd = doublet of doublet of doublets, bs = broad singlet, m = multiplet, coupling constant (Hz), and integration]. High-resolution mass spectra (HRMS) were measured using an Agilent 6230 Accurate-Mass time-of-flight mass spectrometer with a Jet stream electrospray ionization source. Analytical reverse-phase (Sunfire C_{18}; 4.6 mm × 50 mm, 5 mL) high-performance liquid chromatography (HPLC) was performed with a Gilson HPLC equipped with UV and a mass detector. All final compounds were found to be >95% pure by HPLC analysis.

Synthesis of LJL-1. *Boc-Leu-Phe-OMe (1).* To a stirred solution of acid Boc-Leu-OH (1 g, 4.3 mmol, 1 equiv) in dry DCM at r.t. under N_2, methyl ester MeO-Phe-NH_3Cl (1 g, 4.3 mmol, 1 equiv) and TBTU (1.5 g, 4.8 mmol, 1.1 equiv) were added and the resulting solution was stirred for 2 h. 3.14 mL of DIPEA (2.35 g, 18.1 mmol, 4.2 equiv) was then added dropwise, and the resulting mixture was stirred for 15 min. The organic extract was washed with H_2O, brine, then dried over Na_2SO_4, filtered and concentrated *in vacuo*. Purification by silica gel column chromatography (30−35% EtOAc in Hexane) provided the title compound (1.141 g, 2.91 mmol, 67%) as a white solid powder. ^{1}H NMR (600 MHz, $CDCl_3$) δ 7.29−7.19 (m, 3H), 7.10 (d, J = 7.4 Hz, 2H), 6.56 (d, J = 7.8 Hz, 1H), 4.85 (dt, J = 19.9, 7.2 Hz, 2H), 4.10 (d, J = 14.4 Hz, 1H), 3.69 (s, 3H), 3.10 (ddd, J = 41.3, 14.0, 6.0 Hz, 2H), 1.67−1.55 (m, 2H), 1.42 (s, 10H), 0.89 (q, J = 6.0 Hz, 6H)

https://doi.org/10.1021/acsomega.4c04316
ACS Omega 2024, 9, 34829−34840

ppm. HRMS (ES+): calcd for $C_{21}H_{32}N_2O_5$ $[M + Na]^+$, 415.2203; found, 415.2203.

*H_3N-Leu-Phe-OMe (**2**).* A solution of **2** (0.580 g, 1.5 mmol, 1.00 equiv) in TFA (2.5 mL) was stirred at r.t. for several minutes until generation of CO_2 in the reaction mixture was no longer visible. A steady stream of N_2 was used to remove all volatiles and the resulting material was used directly for the next step without further purification.

*Boc-Homophe-Leu-Phe-OMe (**3**).* To a solution of **2** (0.995 g, 2.9 mmol, 1.00 equiv) in dry DCM (29 mL) at r.t. under N_2, DIPEA (1.6 g, 12.2 mmol, 4.2 equiv) was added dropwise, and the reaction mixture was stirred for 15 min. Boc-Homophe-OH (0.811 g, 2.9 mmol, 1 equiv) and TBTU (1.0 g, 3.2 mmol, 1.1 equiv) was added and the solution was stirred for 5 h at r.t. The reaction was quenched with H_2O and washed with brine. The organic layer was then dried over Na_2SO_4, filtered and concentrated *in vacuo*. Purification by silica gel column chromatography (40−50% EtOAc in Hexane) provided the title compound (0.760 g, 1.37 mmol, 47%) as a white solid powder. ^{1}H NMR (600 MHz, $CDCl_3$) δ 7.29−7.24 (m, 2H), 7.24−7.14 (m, 6H), 7.10−7.05 (m, 2H), 6.68 (d, J = 7.9 Hz, 1H), 6.59 (d, J = 8.0 Hz, 1H), 5.16−5.09 (m, 1H), 4.81 (dt, J = 7.9, 6.1 Hz, 1H), 4.43 (td, J = 8.5, 4.9 Hz, 1H), 4.11−4.03 (m, 1H), 3.67 (s, 3H), 3.14−3.01 (m, 2H), 2.64 (t, J = 8.0 Hz, 2H), 2.13−2.01 (m, 1H), 1.89 (dq, J = 13.8, 7.9 Hz, 1H), 1.66−1.56 (m, 2H), 1.54−1.47 (m, 1H), 1.44 (s, 10H), 0.88 (dd, J = 12.4, 6.0 Hz, 6H) ppm. HRMS (ES+): calcd for $C_{31}H_{44}N_3O_6$ $[M + H]^+$, 554.3225; found, 554.3232.

*Boc-Homophe-Leu-Phe-Hydrazide (**4**).* To a solution of **3** (0.357 g, 0.65 mmol, 1 equiv) in MeOH (14.2 mL) at r.t. under N_2, a solution of hydrazine monohydrate (1.957 g, 39 mmol, 61 equiv) was added dropwise and heated at reflux for 2 h. The reaction mixture was then diluted with 40 mL toluene and the remaining solvent was removed by rotary evaporation obtaining the title product, which was used directly without further purification. (0.260 g, 0.460 mmol, 72%) ^{1}H NMR (600 MHz, $CDCl_3$) δ 9.19 (s, 1H), 8.11 (d, J = 8.4 Hz, 1H), 7.82 (d, J = 8.5 Hz, 1H), 7.36 (t, J = 7.5 Hz, 2H), 7.27−7.23 (m, 8H), 7.19−7.14 (m, 2H), 4.51 (td, J = 8.4, 5.6 Hz, 1H), 4.40 (td, J = 9.1, 5.0 Hz, 1H), 4.26 (s, 1H), 3.99 (td, J = 8.5, 5.2 Hz, 1H), 2.98 (dd, J = 13.8, 5.7 Hz, 1H), 2.86 (dd, J = 13.8, 8.6 Hz, 1H), 2.67 (ddd, J = 15.4, 10.6, 5.2 Hz, 1H), 2.62−2.54 (m, 3H), 1.95−1.87 (m, 1H), 1.83 (q, J = 4.8 Hz, 1H), 1.64 (p, J = 6.6 Hz, 1H), 1.47 (s, 9H), 0.91 (dd, J = 21.6, 6.6 Hz, 6H) ppm. HRMS (ES+): calcd for $C_{30}H_{44}N_5O_5$ $[M + H]^+$, 554.3337; found, 554.3340.

*H_3N-Leu-Epoxyketone (**5**).* A solution of Boc-L-Leucine epoxyketone (Combi-Blocks #QM-8198) (0.580 g, 2.14 mmol, 1.00 equiv) in TFA (3.3 mL) was stirred at r.t. for several minutes until generation of CO_2 in the reaction mixture was no longer visible. A steady stream of N_2 was used to remove all volatiles, and the resulting material was used directly for the next step without further purification.

*Boc-Homophe-Leu-Phe-Leu-Ep (**6**).* To a solution of **5** (0.100 g, 0.181 mmol, 1 equiv) in dry DMF under N_2 and at −30 °C, a solution of 43 μL 4 M HCl in dioxane (0.017 g, 0.470 mmol, 2.6 equiv) and *tert*-butyl nitrite (0.022 g, 0.217 mmol, 1.2 equiv) was added and the solution was stirred for 5 h. A solution of **6** (0.057 g, 0.199 mmol, 1.1 equiv) in 200 μL of dry DMF was then added dropwise to the reaction mixture followed by a dropwise addition of DIPEA (0.117 g, 0.903 mmol, 5 equiv) and the resulting mixture was stirred overnight allowing the mixture to rise to r.t. The reaction mixture was first quenched by the addition of water, followed by organic extraction by DCM, and the remaining organic solvent was concentrated in vacuo providing the title compound (0.090 g, 0.331 mmol, 90%). ^{1}H NMR (600 MHz, $CDCl_3$) δ 7.35 (s, 1H), 7.21 (t, J = 7.4 Hz, 2H), 7.17−6.99 (m, 9H), 6.93 (s, 1H), 5.46 (d, J = 7.6 Hz, 1H), 4.83 (q, J = 7.6 Hz, 1H), 4.57 (td, J = 9.1, 3.8 Hz, 2H), 4.24−4.13 (m, 1H), 3.24 (d, J = 5.1 Hz, 1H), 3.06−2.97 (m, 1H), 2.93 (dd, J = 14.0, 7.6 Hz, 1H), 2.82 (d, J = 4.9 Hz, 1H), 2.69−2.53 (m, 2H), 2.02−1.84 (m, 2H), 1.54 (ddt, J = 15.4, 7.9, 3.9 Hz, 3H), 1.48 (s, 4H), 1.45 (s, 11H), 0.89−0.79 (m, 12H) ppm. HRMS (ES+): calcd for C_{39} H_{57} N_4 O_7 $[M + H]^+$, 693.4222; found, 693.4228.

*H_3N-Homophe-Leu-Phe-Leu-Ep (**7**).* A solution of **6** (0.050 g, 0.072 mmol, 1.00 equiv) in TFA (0.11 mL) was stirred at r.t. for several minutes until generation of CO_2 in the reaction mixture was no longer visible. A steady stream of N_2 was used to remove all volatiles and the resulting material was used directly for the next step without further purification.

*Alkyne-Homophe-Leu-Phe-Leu-Ep, LJL-1 (**8**).* To a solution of HBTU (0.025 g, 0.065 mmol, 1.2 equiv) in dry DCM (0.337 mL) at r.t. under N_2, 38 μL DIPEA (0.028 g, 0.220 mmol, 4 equiv) and 6-heptynoic acid (0.008 g, 0.065 mmol, 1.2 equiv) were added and the resulting mixture was stirred for 15 min. Afterward, a solution of **7** (0.038 g, 0.054 mmol, 1 equiv) in 1 mL of dry DCM was added dropwise, and, after the addition, the reaction mixture was stirred for 5 h. The reaction was quenched with H_2O, and washed with brine. The organic layer was then dried over Na_2SO_4, filtered and concentrated *in vacuo*. Purification by reverse phase HPLC afforded the title compound as a white solid (0.015 g, 0.021 mmol, 40%). ^{1}H NMR (600 MHz, $CDCl_3$) δ 8.37 (d, J = 111.5 Hz, 1H), 7.85 (s, 1H), 7.51 (s, 1H), 7.06 (d, J = 7.1 Hz, 4H), 7.00−6.90 (m, 6H), 6.85 (d, J = 7.5 Hz, 1H), 5.08 (d, J = 52.5 Hz, 3H), 4.66 (td, J = 9.3, 3.7 Hz, 1H), 3.22−3.15 (m, 1H), 3.03−2.86 (m, 2H), 2.82 (d, J = 4.7 Hz, 1H), 2.55 (td, J = 21.9, 6.7 Hz, 2H), 2.34 (ddt, J = 42.9, 14.5, 7.6 Hz, 2H), 2.26−2.20 (m, 2H), 1.99−1.85 (m, 3H), 1.85−1.72 (m, 3H), 1.72−1.64 (m, 1H), 1.64−1.52 (m, 4H), 1.48 (s, 3H), 1.47−1.42 (m, 1H), 0.84 (ddd, J = 17.7, 6.6, 3.9 Hz, 12H) ppm. ^{13}C NMR (150 MHz, $CDCl_3$) δ (ppm) 172.97, 171.88, 171.76, 171.32, 155.41, 141.30, 136.36, 129.29, 128.49, 128.37, 128.28, 126.02, 84.30, 81.97, 68.77, 67.17, 64.16, 58.81, 49.34, 42.71, 40.14, 35.80, 32.18, 28.23, 25.33, 25.18, 25.06, 23.31, 22.40, 21.83, 18.42, 16.72. HRMS (ES+): calcd for $C_{41}H_{57}N_4O_6$ $[M + H]^+$, 701.4273; found, 701.4272.

Synthesis of LJL-2. *Boc-Phe-Leu-Ep (**9**).* To a solution of Boc-Phe-OH (0.254 g, 0.956 mmol, 1 equiv) in dry DCM (1.90 mL) at r.t. under N_2, DIPEA (0.097 g, 0.75 mmol, 4 equiv) was added dropwise, and the reaction mixture was stirred for 15 min. **5** (0.300 g, 1.1 mmol, 1.1 equiv) and TBTU (0.368 g, 1.2 mmol, 1.2 equiv) was added and the solution was stirred for 5 h at r.t.. The reaction was quenched with H_2O, and washed with brine. The organic layer was then dried over Na_2SO_4, filtered and concentrated *in vacuo*. Purification by silica gel column chromatography (20−40% EtOAc in Hexane) provided the title compound (0.032 g, 0.076 mmol, 41%) as a white solid powder. ^{1}H NMR (600 MHz, $CDCl_3$) δ 7.31−7.16 (m, 5H), 6.20 (d, J = 8.2 Hz, 1H), 4.96 (s, 1H), 4.57 (ddd, J = 11.0, 8.2, 3.2 Hz, 1H), 4.32 (s, 1H), 3.24 (s, 1H), 3.03 (qd, J = 14.0, 6.8 Hz, 2H), 2.88 (d, J = 5.0 Hz, 1H), 1.49 (s, 3H), 1.47−1.43 (m, 1H), 1.41 (s, 10H), 1.17 (ddd, J = 13.9, 10.3, 4.0 Hz, 1H), 0.92 (d, J = 6.4 Hz, 3H), 0.87 (d, J =

https://doi.org/10.1021/acsomega.4c04316
ACS Omega 2024, 9, 34829−34840

6.5 Hz, 3H) ppm. HRMS (ES+): calcd for $C_{23}H_{35}N_2O_5$ $[M + H]^+$, 419.2540; found, 419.2540.

*H_3N-Phe-Leu-Ep (**10**).* A solution of **9** (0.058 g, 0.15 mmol, 1.00 equiv) in TFA (0.21 mL) was stirred at r.t. for several minutes until generation of CO_2 in the reaction mixture was no longer visible. A steady stream of N_2 was used to remove all volatiles and the resulting material was used directly for the next step without further purification.

*1-(1H-Imidazol-1-yl)hept-6-yn-1-one (**11**).* To a solution of 6-heptynoic acid (0.997 g, 7.9 mmol, 1 equiv) in dry DCM (19 mL) at r.t. under N_2, carbonyldiimidazole (1.5 g, 9.5 mmol, 1.2 equiv) was added in one portion and the reaction mixture was stirred at r.t. overnight. Purification by silica gel column chromatography (60−65% EtOAc in hexane) provided the title compound (0.993 g, 5.636 mmol, 71%) as a white solid powder. ^{1}H NMR (600 MHz, $CDCl_3$) δ 8.17 (s, 1H), 7.46 (t, J = 1.5 Hz, 1H), 7.10−7.06 (m, 2H), 2.89 (t, J = 7.3 Hz, 2H), 2.25 (m, 2H), 1.96 (t, J = 2.7 Hz, 1H), 1.91 (q, J = 7.5 Hz, 2H), 1.68−1.61 (m, 2H) ppm. HRMS (ES+): calcd for $C_{10}H_{13}N_2O$ $[M + H]^+$, 177.1022; found, 177.1019.

*Alkyne-Phe-Leu-Ep, LJL-2 (**12**).* To a solution of **9** (0.058 g, 0.130 mmol, 1 equiv) in dry DCM at r.t. under N_2, **11** (0.026 g, 0.150 mmol, 1.1 equiv) was added in one portion, and 28 μL DIPEA (0.021 g, 0.160 mmol, 1.2 equiv) was added dropwise. The reaction mixture was stirred at r.t. for 5 h. The reaction was then quenched with H_2O, and washed with brine. The organic layer was then dried over Na_2SO_4, filtered and concentrated *in vacuo*. Purification by HPLC and lyophilization afforded the title compound (0.019 g, 0.045 mmol, 33%) as an off-white solid. ^{1}H NMR (600 MHz, $CDCl_3$) δ 7.36−7.27 (m, 3H), 7.24−7.19 (m, 2H), 6.08 (dd, J = 13.3, 7.6 Hz, 2H), 4.66 (q, J = 7.3 Hz, 1H), 4.51 (ddd, J = 10.6, 7.7, 3.1 Hz, 1H), 3.21 (d, J = 5.0 Hz, 1H), 3.03 (qd, J = 14.0, 7.1 Hz, 2H), 2.89 (dd, J = 5.0, 2.6 Hz, 1H), 2.17 (dtd, J = 9.5, 7.2, 2.1 Hz, 5H), 1.94 (dt, J = 5.5, 2.7 Hz, 1H), 1.73−1.65 (m, 2H), 1.50 (s, 3H), 1.49−1.44 (m, 2H), 0.89 (dd, J = 16.4, 6.4 Hz, 6H) ppm. ^{13}C NMR (150 MHz, DMSO-d_6) δ (ppm) 208.30, 171.76, 171.67, 137.87, 129.11, 127.94, 126.17, 84.31, 71.13, 58.89, 53.12, 51.58, 49.50, 38.44, 37.61, 34.46, 27.19, 24.54, 24.24, 23.16, 21.05, 17.39, 16.47. HRMS (ES+): calcd for $C_{25}H_{35}N_2O_4$ $[M + H]^+$, 427.2591; found, 427.2587.

Cell Culture. HEK293[58,59] and HepG2[60] cells were cultured in DMEM supplemented with 10% heat-inactivated fetal bovine serum (FBS) and 1% penicillin-streptomycin. Cells were grown in T75 cell culture flasks maintained at 37 °C in 5% CO_2, and passaged at 60−80% cell confluence.

L. donovani MHOM/ET/67/HU3 promastigotes were grown axenically at 28 °C in M199 containing 40 mM HEPES, 0.1 mM adenine, 0.0001% biotin, 4.62 mM $NaHCO_3$, 10% heat-inactivated FBS and 1% streptomycin/penicillin in T25 cell culture flasks. The cultures were diluted every 3−4 days to maintain the parasite density between 10^6 and 4×10^7 parasites/mL, as determined microscopically with a hemocytometer.[61]

T. vaginalis F1623 trophozoites were grown in TYM (trypticase, yeast extract, maltose)-Diamond's medium supplemented with 180 mM ammonium iron(II) sulfate at 37 °C under anaerobic conditions. Trophozoites were seeded at approximately 1×10^5 cells/mL into 25 mL universal bottles, which were then completely filled and tightly capped for 24 h. Cells were passaged when at a density of ~1×10^6 cells/mL, as determined microscopically with a hemocytometer.[23]

Preparation of Cell Lysates. All cell types in their respective media were centrifuged for 10 min at 24,000*g* and 4 °C. The supernatant was discarded, and the cells resuspended in phosphate-buffered saline (PBS) before undergoing the same centrifugation again. This process was repeated once more. After the final centrifugation, the supernatant was removed and cell pellets were stored at −80 °C.

PBS was used as a lysis buffer and approximately twice the volume was added relative to the volume of the pellet so that a final concentration of 5−10 mg/mL was achieved. Cell lysis was performed on ice using a Qsonica CL-18 sonicator probe set to pulses of 2 s with 5 s rest periods over a total of 44 s. Sonicated samples were centrifuged for 10 min at 11,000*g* and 4 °C. The supernatant was recovered, aliquoted, flash frozen in a dry ice/acetone bath, and stored at −80 °C. Protein concentration was determined using the Pierce BCA Protein Assay kit (Fisher #23227).

HEK293 Cell Viability Assay. Resazurin was used to measure HEK293 cell viability as described previously.[59] All test compounds were dissolved in and diluted using 100% DMSO. Compounds were diluted 3-fold through an eight-point concentration down from 4 μM. Compound (1 μL) was spotted into each well of a clear, flat-bottomed 96-well plate (Fisher #FB012931) followed by addition of 49 μL DMEM medium. Cells were diluted to 4×10^5 cells/mL and 50 μL solution dispensed into each well. Cells were incubated for 48 h at 37 °C in a 5% CO_2 atmosphere. After 48 h, 20 μL 0.5 mM resazurin in PBS was added into each well. Assay plates were incubated in the dark for 2 h at 37 °C and 5% CO_2. Fluorescence was measured at ex/em 531/595 nm in a 2104 EnVision multilabel plate reader.

Human c20S Activity and Inhibition Assays. Inhibitors were first diluted in DMSO so that the final DMSO concentration in each assay well was 2.5%. All other dilutions were prepared in assay buffer containing 50 mM HEPES, 1 mM DTT, pH 7.5. To activate c20S, 4 nM c20S (R&D Systems; E-360) was mixed with 200 nM PA28α (R&D Systems; E-381) in equal volume proportions for one 1 h before addition of inhibitor. To normalize the DMSO concentration, all probes and inhibitors were diluted, 2- or 5-fold, in 100% DMSO before being transferred to wells containing c20S so that the final concentration was 2.5%. This mixture was incubated for 1 h at room temperature (RT) and 4 μL then transferred into 384-well small volume plates (Greiner #784900). Immediately afterward, 4 μL AMC substrate was added to a final concentration of 50 μM. The β1, β2, and β5 activities of c20S were measured using Z-LLE-AMC, Boc-LRR-AMC, and Suc-LLVY-AMC, respectively. The rate of AMC cleavage was measured for 4 h and the potency of each compound was compared to vehicle (DMSO) control. All reactions were performed at 37 °C in triplicate in a final volume of 8 μL. Fluorescence was measured at ex/em 360/460 nm in a Biotek Synergy HTX plate reader. IC_{50} values were calculated using GraphPad Prism 8 by normalizing activity to DMSO controls and interpolating the data using the "Sigmoidal, 4PL, X is log(concentration)" algorithm.

Probe Incubation, Click Chemistry and SDS-PAGE. Each sample (diluted in PBS to 16 μL) contained either 100 ng c20S or 16 μg cell lysate, unless otherwise stated in the figures. Inhibitors were first diluted with 100% DMSO to the appropriate concentration and 1 μL inhibitor or vehicle (DMSO) was added into each sample and incubated for 1 h at 37 °C. Afterward, 1 μL probe was diluted in 100% DMSO so

https://doi.org/10.1021/acsomega.4c04316
ACS Omega 2024, 9, 34829−34840

that the final concentration was 2 μM for Me_4BodipyFL-Ahx_3L_3VS with all three cell extracts, 10 μM for LJL-1 and LJL-2 with the *L. donovani* extracts, and 2 μM LJL-1 and LJL-2 with the *T. vaginalis* and HepG2 extracts. Probes were coincubated with each sample for 3 h at 37 °C.

Samples requiring click chemistry, using a starting volume 18 μL, were denatured using 2.5 μL 1% SDS in PBS and briefly vortexed. To achieve a final concentration 1.5-fold greater than the alkyne, TAMRA biotin azide (Vector Laboratories #CCT-1048) was diluted in 100% DMSO and 0.5 μL was added to the sample. Next, 2.5 μL of the copper catalyst mixture was freshly prepared; specifically, a 3:1:1 ratio of 1.7 mM TBTA (in 20% DMSO in *t*-butanol), 50 mM $CuSO_4$ (in water) and 50 mM TCEP (in water and adjusted to pH 7.0 using 1 M NaOH). This sample mixture, now 23.5 μL, was left for 30 min at 37 °C.

Next, 8 μL 4× Bolt LDS sample buffer (Fisher #B0007) containing 250 mM DTT was added to each sample and boiled for 5 min at 95 °C. Samples were quickly centrifuged and placed into precast 10-, 15- or 17-well Bolt 1.0 mm, 4−12% Bis-Tris Plus mini protein gels (Fisher #NW04120BOX, NW04125BOX, NW04127BOX). Gels were placed in an Invitrogen mini gel tank (Fisher #A25977) containing 1× MOPS running buffer (Fisher #NP000102) at the designated volume. The last lane on either side of the gel was loaded with 1.5 μL PageRuler prestained protein ladder (Fisher #26616). Gels were first electrophoresed at 60 V until the dye front had migrated about 15% of the way though the gel, at which point, the voltage was increased to 120 V for the duration of electrophoresis. Gels were washed with water after electrophoresis and fixed for 5 min in 6:3:1 water/ethanol/acetic acid. Fluorescent imaging was performed using a Bio-Rad ChemiDoc MP Imaging System with the settings optimized to visualize Qdots 525 (Bodipy) or Alexa 546 (TAMRA).

Affinity Purification. To 500 μL 2 mg/mL lysate, 10 μL inhibitor(s) or vehicle (DMSO) was added and the lysate incubated for 1 h at 37 °C. Next, 10 μM (10 μL) LJL-1 for*L. donovani*and 2 μM LJL-2 for*T. vaginalis*, was added to the lysate and incubated for 1 h at 37 °C. Proteins were denatured by adding 62.5 μL of 1% SDS in PBS followed by brief vortexing. Click chemistry was initiated by adding 62.5 μL of the copper catalyst mixture to 12.5 μL TAMRA biotin azide (final concentrations of 15 and 3 μM for*L. donovani* and*T. vaginalis*, respectively) followed by a 30 min incubation at 37 °C.

After incubation, the lysate was precipitated using three volumes of cold acetone and standing in a −20 °C freezer for 30 min. The precipitated protein sample was centrifuged at 11,000*g* and 4 °C for 5 min to generate a pellet and the supernatant was aspirated. The protein pellet was washed three times with cold acetone. In each wash cycle, the supernatant was aspirated, the pellet resuspended in cold acetone and centrifuged. After the final wash step, the supernatant was aspirated, and the protein pellet was left to air-dry. Once dried, the pellet was resuspended in 250 μL 1% SDS in PBS and vortexed. The resuspended sample was centrifuged at 11,000*g* and 4 °C for 5 min and the supernatant was retained, while any insoluble proteins in the pellet were discarded. This supernatant was added to 75 μL NeutrAvidin Agarose resin (Fisher #PI29200) and rotated overnight at r.t. on an end-over-end Labquake Shaker/Rotisserie. The following day, this suspension was transferred onto a Bio-Rad Micro Bio-Spin column (Bio-Rad #7326204) and centrifuged at 11,000*g* for 30 s. The beads were washed 5 times with each of the following: (1) 4 M Urea, 250 mM NaCl and 2% SDS; (2) 8 M urea; and (3) 50 mM ammonium bicarbonate. After the final wash, the beads were transferred into a separate microfuge tube and 40 μL 4× Bolt LDS sample buffer containing 250 mM DTT was added. Each sample was boiled for 15 min at 95 °C to disrupt biotin-neutravidin binding. Samples were quickly centrifuged and the supernatant placed into precast 15 well Bolt 1.0 mm, 4−12% Bis-Tris Plus mini protein gels. Electrophoresis, gel fixation and fluorescence visualization were as described above.

In Gel Trypsin Digest. The protocol published by Shevchenko et al.[62] was used for in-gel trypsin digestion of all protein bands of interest.

Proteomic Sample Preparation and Analysis. Tryptic samples were desalted using custom-made C18 spin tips by packing Empore C18 extraction disks (Fisher #13−110−019) into P1000 pipet tips. C18 tips were placed into centrifuge adapters (GL sciences #5010−21514) and then into 2 mL microfuge tubes. P1000 pipet tips were trimmed at the largest end so that they would fit inside a benchtop centrifuge.

C18 was equilibrated with 150 μL liquid chromatography-mass spectrometry (LC-MS) grade ACN and centrifuged at 400*g* for 1 min at RT. Next, 150 μL 0.1% TFA in LC-MS grade water was centrifuged through the tips at 400*g* for 2 min at r.t. twice. During centrifugation, the proteomic sample(s) were acidified with TFA to achieve a final pH < 3.0. Afterward, the acidified sample was transferred to the C18 tip and centrifuged at 400*g* for 4 min or until all the liquid eluted through the tip. The C18 was centrifuged using 150 μL 0.1% TFA in LC-MS grade water at 400*g* for 4 min. This was repeated 4 times. After the final wash, the microfuge vials were replaced with max recovery tubes and the peptides were eluted using 150 μL 0.1% TFA in 50% ACN in water and centrifuged at 400*g* for 4 min for two cycles. Lastly, 150 μL 0.1% TFA in 80% ACN in water was centrifuged once at 400*g* for 4 min. Approximately 450 μL sample was then placed in a rotary evaporator until dryness and stored at −80 °C.

Proteome analysis was performed using an Easy—nLC coupled to an Orbitrap Eclipse mass spectrometer (Thermo Fisher Scientific). The 71 min method, 60 min effective gradient of solvent A (2% ACN, 0.1% FA) to solvent B (80% ACN, 0.1% FA) started at 3 to 23% B over 45 min; from 23 to 40% B over 15 min; from 40 to 95% B over one min and holding for 10 min. The flow rate was 200 nL/min. The Orbitrap Eclipse mass spectrometer was performed in positive mode. MS1 spectra were scanned in a range of 375−1500 m/z, at a resolution of 60,000, with a maximum injection time (max IT) in automatic mode, and an AGC target in standard mode. The data acquisition mode was set with a time between master scans of 3 s. The MS2 quadrupole isolation mode had an isolation width of 0.7 m/z. The MS2 spectra scanned range was set in auto mode with a resolution of 15,000. The AGC target was set at 400% with a maximum injection time of 22 ms. The normalized collision energy was set to 30%. Dynamic exclusion was set at 60 s.

RAW data were processed using Peaks 8.5 (Bioinformatics Solutions Inc.). MS2 data were searched against either the*L. donovani* (Proteome ID: UP000008980) or the*T. vaginalis* (Proteome ID: UP000001542) proteome. A precursor tolerance of 20 ppm and 0.01 Da for MS2 fragments was defined. Trypsin was used for protease digestion. Data were filtered to a 1% peptide false discovery rate with the target-

https://doi.org/10.1021/acsomega.4c04316
ACS Omega 2024, 9, 34829−34840

decoy strategy. Peptides were subjected to bylabel-free quantification.

■ ASSOCIATED CONTENT

Data Availability Statement

L. donovani proteins identified bylabel-free MS quantification using LJL-1, *T. vaginalis* proteins identified bylabel-free MS quantification using LJL-2 and the RAW files for all proteomic analysis can be found on: ftp://massive.ucsd.edu/v07/MSV000094658/.

Supporting Information

The Supporting Information is available free of charge at https://pubs.acs.org/doi/10.1021/acsomega.4c04316.

1H NMR spectra and HR-MS for most compounds and associated gel, cell viability and c20S inhibition assays (PDF)

■ AUTHOR INFORMATION

Corresponding Authors

Anthony J. O'Donoghue − *Center for Discovery and Innovation in Parasitic Diseases, Skaggs School of Pharmacy and Pharmaceutical Sciences, University of California, San Diego, La Jolla, California 92093, United States;* orcid.org/0000-0001-5695-0409; Email: ajodonoghue@health.ucsd.edu

Conor R. Caffrey − *Center for Discovery and Innovation in Parasitic Diseases, Skaggs School of Pharmacy and Pharmaceutical Sciences, University of California, San Diego, La Jolla, California 92093, United States;* orcid.org/0000-0003-3048-8572; Email: ccaffrey@health.ucsd.edu

Authors

Lawrence J. Liu − *Department of Chemistry and Biochemistry, University of California San Diego, La Jolla, California 92093, United States; Center for Discovery and Innovation in Parasitic Diseases, Skaggs School of Pharmacy and Pharmaceutical Sciences, University of California, San Diego, La Jolla, California 92093, United States;* orcid.org/0000-0003-2811-1274

Bobby Lucero − *Department of Chemistry and Biochemistry, University of California San Diego, La Jolla, California 92093, United States; Center for Discovery and Innovation in Parasitic Diseases, Skaggs School of Pharmacy and Pharmaceutical Sciences, University of California, San Diego, La Jolla, California 92093, United States*

Cindy Manriquez-Rodriguez − *Center for Autoimmunity and Inflammation, La Jolla Institute for Immunology, La Jolla, California 92037, United States; Laboratory for Immunochemical Circuits, La Jolla Institute for Immunology, La Jolla, California 92037, United States*

Karol R. Francisco − *Center for Discovery and Innovation in Parasitic Diseases, Skaggs School of Pharmacy and Pharmaceutical Sciences, University of California, San Diego, La Jolla, California 92093, United States*

Thaiz R. Teixeira − *Center for Discovery and Innovation in Parasitic Diseases, Skaggs School of Pharmacy and Pharmaceutical Sciences, University of California, San Diego, La Jolla, California 92093, United States*

Darius J. Yohannan − *Department of Chemistry and Biochemistry, University of California San Diego, La Jolla, California 92093, United States; Center for Discovery and Innovation in Parasitic Diseases, Skaggs School of Pharmacy and Pharmaceutical Sciences, University of California, San Diego, La Jolla, California 92093, United States;* orcid.org/0009-0007-0394-8234

Carlo Ballatore − *Department of Chemistry and Biochemistry, University of California San Diego, La Jolla, California 92093, United States; Center for Discovery and Innovation in Parasitic Diseases, Skaggs School of Pharmacy and Pharmaceutical Sciences, University of California, San Diego, La Jolla, California 92093, United States*

Samuel A. Myers − *Center for Autoimmunity and Inflammation, La Jolla Institute for Immunology, La Jolla, California 92037, United States; Laboratory for Immunochemical Circuits, La Jolla Institute for Immunology, La Jolla, California 92037, United States*

Complete contact information is available at: https://pubs.acs.org/10.1021/acsomega.4c04316

Notes

The authors declare no competing financial interest.

■ ACKNOWLEDGMENTS

The research was supported by NIH grants R21AI171824 to A.J.O. and C.R.C., and R01AI158612 to A.J.O. Additional support was obtained from Department of Defense (W81XWH2210520 to David Fidock and Matt Bogyo with a subaward to A.J.O. as Site PI). HR-MS data were collected at the UC San Diego Chemistry and Biochemistry Molecular Mass Spectrometry Facility (MMSF). NMR spectra were collected at the UC San Diego Skaggs School of Pharmacy and Pharmaceutical Sciences NMR Facility. We thank Jair Lage De Siqueira-Neto and Miriam Giardini for providing*L. donovani* pellets, Lars Eckmann and Yukiko Miyamoto for the*T. vaginalis* lysate, and Elizabeth Winzeler for the HepG2 cell culture.

■ ACRONYMS

c20Sconstitutive 20S proteasome
Ld20S*Leishmania donovani* 20S proteasome
Tv20S*Trichomonas vaginalis* 20S proteasome
PMSFphenylmethylsulfonyl fluoride
CPcarmaphycin
ABPactivity-based probe
MZBmarizomib
BTZbortezomib
CFZcarfilzomib
RPregulatory particle
UPSubiquitin proteasome system
PIproteasome inhibitor
TAMRA5-carboxytetramethylrhodamine

■ REFERENCES

(1) Thibaudeau, T. A.; Smith, D. M. A Practical Review of Proteasome Pharmacology. *Pharmacol. Rev.* **2019**, *71* (2), 170−197.

(2) Ciechanover, A.; Schwartz, A. L. The ubiquitin-proteasome pathway: the complexity and myriad functions of proteins death. *Proc. Natl. Acad. Sci. U.S.A.* **1998**, *95* (6), 2727−2730.

(3) Saha, A.; Oanca, G.; Mondal, D.; Warshel, A. Exploring the Proteolysis Mechanism of the Proteasomes. *J. Phys. Chem. B* **2020**, *124* (27), 5626−5635.

(4) Adams, J. The development of proteasome inhibitors as anticancer drugs. *Cancer Cell* **2004**, *5* (5), 417−421.

(5) Kopp, F.; Hendil, K. B.; Dahlmann, B.; Kristensen, P.; Sobek, A.; Uerkvitz, W. Subunit arrangement in the human 20S proteasome. *Proc. Natl. Acad. Sci. U.S.A.* **1997**, *94* (7), 2939−2944.

(6) Moore, B. S.; Eustáquio, A. S.; McGlinchey, R. P. Advances in and applications of proteasome inhibitors. *Curr. Opin. Chem. Biol.* **2008**, *12* (4), 434−440.
(7) Collins, G. A.; Goldberg, A. L. The Logic of the 26S Proteasome. *Cell* **2017**, *169* (5), 792−806.
(8) Groen, K.; van de Donk, N.; Stege, C.; Zweegman, S.; Nijhof, I. S. Carfilzomib for relapsed and refractory multiple myeloma. *Cancer Manage. Res.* **2019**, *11*, 2663−2675.
(9) Chen, D.; Frezza, M.; Schmitt, S.; Kanwar, J.; Dou, Q. P. Bortezomib as the first proteasome inhibitor anticancer drug: current status and future perspectives. *Curr. Cancer Drug Targets* **2011**, *11* (3), 239−253.
(10) Shirley, M. Ixazomib: First Global Approval. *Drugs* **2016**, *76* (3), 405−411.
(11) Bibo-Verdugo, B.; Wang, S. C.; Almaliti, J.; Ta, A. P.; Jiang, Z.; Wong, D. A.; Lietz, C. B.; Suzuki, B. M.; El-Sakkary, N.; Hook, V.; et al. The Proteasome as a Drug Target in the Metazoan Pathogen, Schistosoma mansoni. *ACS Infect. Dis.* **2019**, *5* (10), 1802−1812.
(12) O'Donoghue, A. J.; Bibo-Verdugo, B.; Miyamoto, Y.; Wang, S. C.; Yang, J. Z.; Zuill, D. E.; Matsuka, S.; Jiang, Z.; Almaliti, J.; Caffrey, C. R.; et al. 20S Proteasome as a Drug Target in Trichomonas vaginalis. *Antimicrob. Agents Chemother.* **2019**, *63* (11), No. e00448-19, DOI: 10.1128/AAC.00448-19.
(13) Jalovecka, M.; Hartmann, D.; Miyamoto, Y.; Eckmann, L.; Hajdusek, O.; O'Donoghue, A. J.; Sojka, D. Validation of Babesia proteasome as a drug target. *Int. J. Parasitol.: Drugs Drug Resist.* **2018**, *8* (3), 394−402.
(14) Caffrey, C. R.; Steverding, D.; Ferreira, R. S.; de Oliveira, R. B.; O'Donoghue, A. J.; Monti, L.; Ballatore, C.; Bachovchin, K. A.; Ferrins, L.; Pollastri, M. P.et al. Drug Discovery and Development for Kinetoplastid Diseases. In *Burger's Medicinal Chemistry and Drug Discovery*; John Wiley & Sons, 2003; p 79.
(15) Xie, S. C.; Gillett, D. L.; Spillman, N. J.; Tsu, C.; Luth, M. R.; Ottilie, S.; Duffy, S.; Gould, A. E.; Hales, P.; Seager, B. A.; et al. Target Validation and Identification of Novel Boronate Inhibitors of the *Plasmodium falciparum* Proteasome. *J. Med. Chem.* **2018**, *61* (22), 10053−10066.
(16) Li, H.; O'Donoghue, A. J.; van der Linden, W. A.; Xie, S. C.; Yoo, E.; Foe, I. T.; Tilley, L.; Craik, C. S.; da Fonseca, P. C.; Bogyo, M. Structure- and function-based design of Plasmodium-selective proteasome inhibitors. *Nature* **2016**, *530* (7589), 233−236.
(17) Zhang, H.; Ginn, J.; Zhan, W.; Liu, Y. J.; Leung, A.; Toita, A.; Okamoto, R.; Wong, T. T.; Imaeda, T.; Hara, R.; et al. Design, Synthesis, and Optimization of Macrocyclic Peptides as Species-Selective Antimalaria Proteasome Inhibitors. *J. Med. Chem.* **2022**, *65* (13), 9350−9375.
(18) LaMonte, G. M.; Almaliti, J.; Bibo-Verdugo, B.; Keller, L.; Zou, B. Y.; Yang, J.; Antonova-Koch, Y.; Orjuela-Sanchez, P.; Boyle, C. A.; Vigil, E.; et al. Development of a Potent Inhibitor of the Plasmodium Proteasome with Reduced Mammalian Toxicity. *J. Med. Chem.* **2017**, *60* (15), 6721−6732.
(19) Wyllie, S.; Brand, S.; Thomas, M.; De Rycker, M.; Chung, C. W.; Pena, I.; Bingham, R. P.; Bueren-Calabuig, J. A.; Cantizani, J.; Cebrian, D.; et al. Preclinical candidate for the treatment of visceral leishmaniasis that acts through proteasome inhibition. *Proc. Natl. Acad. Sci. U.S.A.* **2019**, *116* (19), 9318−9323.
(20) Khare, S.; Nagle, A. S.; Biggart, A.; Lai, Y. H.; Liang, F.; Davis, L. C.; Barnes, S. W.; Mathison, C. J.; Myburgh, E.; Gao, M. Y.; et al. Proteasome inhibition for treatment of leishmaniasis, Chagas disease and sleeping sickness. *Nature* **2016**, *537* (7619), 229−233.
(21) Nagle, A.; Biggart, A.; Be, C.; Srinivas, H.; Hein, A.; Caridha, D.; Sciotti, R. J.; Pybus, B.; Kreishman-Deitrick, M.; Bursulaya, B.; et al. Discovery and Characterization of Clinical Candidate LXE408 as a Kinetoplastid-Selective Proteasome Inhibitor for the Treatment of Leishmaniases. *J. Med. Chem.* **2020**, *63* (19), 10773−10781.
(22) Jiang, Z.; Silva, E. B.; Liu, C.; Fajtová, P.; Liu, L. J.; El-Sakkary, N.; Skinner, D. E.; Syed, A.; Wang, S. C.; Caffrey, C. R. et al. Development of subunit selective proteasome substrates for Schistosoma species *bioRxiv* 2024.
(23) Fajtova, P.; Hurysz, B. M.; Miyamoto, Y.; Serafim, M.; Jiang, Z.; Trujillo, D. F.; Liu, L.; Somani, U.; Almaliti, J.; Myers, S. A. et al. Development of subunit selective substrates for Trichomonas vaginalis proteasome *bioRxiv* 2023 DOI: 10.1101/2023.04.05.535794.
(24) Hua, S.-b.; To, W.-Y.; Nguyen, T. T.; Wong, M.-L.; Wang, C. C. Purification and characterization of proteasomes from Trypanosoma brucei. *Mol. Biochem. Parasitol.* **1996**, *78* (1−2), 33−46.
(25) Beyette, J. R.; Hubbell, T.; Monaco, J. J.Purification of 20S Proteasomes. In *Antigen Processing and Presentation Protocols*; Springer, 2000; Vol. *156*, pp 1−16.
(26) Dong, Y.; Zhang, S.; Wu, Z.; Li, X.; Wang, W. L.; Zhu, Y.; Stoilova-McPhie, S.; Lu, Y.; Finley, D.; Mao, Y. Cryo-EM structures and dynamics of substrate-engaged human 26S proteasome. *Nature* **2019**, *565* (7737), 49−55.
(27) Morris, E. P.; da Fonseca, P. C. A. High-resolution cryo-EM proteasome structures in drug development. *Acta Crystallogr., Sect. D: Struct. Biol.* **2017**, *73* (Pt 6), 522−533.
(28) Hewings, D. S.; Flygare, J. A.; Wertz, I. E.; Bogyo, M. Activity-based probes for the multicatalytic proteasome. *FEBS J.* **2017**, *284* (10), 1540−1554.
(29) Verdoes, M.; Florea, B. I.; Menendez-Benito, V.; Maynard, C. J.; Witte, M. D.; van der Linden, W. A.; van den Nieuwendijk, A. M.; Hofmann, T.; Berkers, C. R.; van Leeuwen, F. W.; et al. A fluorescent broad-spectrum proteasome inhibitor for labeling proteasomes in vitro and in vivo. *Chem. Biol.* **2006**, *13* (11), 1217−1226.
(30) Li, H.; van der Linden, W. A.; Verdoes, M.; Florea, B. I.; McAllister, F. E.; Govindaswamy, K.; Elias, J. E.; Bhanot, P.; Overkleeft, H. S.; Bogyo, M. Assessing subunit dependency of the Plasmodium proteasome using small molecule inhibitors and active site probes. *ACS Chem. Biol.* **2014**, *9* (8), 1869−1876.
(31) Türker, F.; Bharadwaj, R. A.; Kleinman, J. E.; Weinberger, D. R.; Hyde, T. M.; White, C. J.; Williams, D. W.; Margolis, S. S. Orthogonal approaches required to measure proteasome composition and activity in mammalian brain tissue. *J. Biol. Chem.* **2023**, *299* (6), No. 104811.
(32) Siqueira-Neto, J. L.; Debnath, A.; McCall, L. I.; Bernatchez, J. A.; Ndao, M.; Reed, S. L.; Rosenthal, P. J. Cysteine proteases in protozoan parasites. *PLoS Neglected Trop. Dis.* **2018**, *12* (8), No. e0006512.
(33) Caffrey, C. R.; Goupil, L.; Rebello, K. M.; Dalton, J. P.; Smith, D. Cysteine proteases as digestive enzymes in parasitic helminths. *PLoS Neglected Trop. Dis.* **2018**, *12*, No. e0005840, DOI: 10.1371/journal.pntd.0005840.
(34) Kolb, H.; Finn, M.; Sharpless, K. Click Chemistry: Diverse Chemical Function from a Few Good Reactions. *Angew. Int., Ed. Chem.* **2001**, *40* (11), 2004−2021, DOI: 10.1002/1521-3773(20010601)40:113.0.CO;2-5.
(35) Huber, E. M.; de Bruin, G.; Heinemeyer, W.; Soriano, G. P.; Overkleeft, H. S.; Groll, M. Systematic Analyses of Substrate Preferences of 20S Proteasomes Using Peptidic Epoxyketone Inhibitors. *J. Am. Chem. Soc.* **2015**, *137* (24), 7835−7842.
(36) Berkers, C. R.; van Leeuwen, F. W.; Groothuis, T. A.; Peperzak, V.; van Tilburg, E. W.; Borst, J.; Neefjes, J. J.; Ovaa, H. Profiling proteasome activity in tissue with fluorescent probes. *Mol. Pharmaceutics* **2007**, *4* (5), 739−748.
(37) Kisselev, A. F.; Garcia-Calvo, M.; Overkleeft, H. S.; Peterson, E.; Pennington, M. W.; Ploegh, H. L.; Thornberry, N. A.; Goldberg, A. L. The caspase-like sites of proteasomes, their substrate specificity, new inhibitors and substrates, and allosteric interactions with the trypsin-like sites. *J. Biol. Chem.* **2003**, *278* (38), 35869−35877.
(38) Geurink, P. P.; van der Linden, W. A.; Mirabella, A. C.; Gallastegui, N.; de Bruin, G.; Blom, A. E.; Voges, M. J.; Mock, E. D.; Florea, B. I.; van der Marel, G. A.; et al. Incorporation of non-natural amino acids improves cell permeability and potency of specific inhibitors of proteasome trypsin-like sites. *J. Med. Chem.* **2013**, *56* (3), 1262−1275.
(39) Muli, C. S.; Trader, D. J. 20S proteasome hydrolysis of LLVY substrates to determine preferences for moieties in its primed substrate channel. *Bioorg. Med. Chem. Lett.* **2023**, *85*, No. 129233.

(40) Lidumniece, E.; Withers-Martinez, C.; Hackett, F.; Collins, C. R.; Perrin, A. J.; Koussis, K.; Bisson, C.; Blackman, M. J.; Jirgensons, A. Peptidic boronic acids are potent cell-permeable inhibitors of the malaria parasite egress serine protease SUB1. *Proc. Natl. Acad. Sci. U.S.A.* **2021**, *118* (20), No. e2022696118, DOI: 10.1073/pnas.2022696118.
(41) Grewal, J. S.; Catta-Preta, C. M. C.; Brown, E.; Anand, J.; Mottram, J. C. Evaluation of clan CD C11 peptidase PNT1 and other Leishmania mexicana cysteine peptidases as potential drug targets. *Biochimie* **2019**, *166*, 150−160.
(42) Wang, G.; Mahesh, U.; Chen, G. Y.; Yao, S. Q. Solid-phase synthesis of peptide vinyl sulfones as potential inhibitors and activity-based probes of cysteine proteases. *Org. Lett.* **2003**, *5* (5), 737−740.
(43) McKerrow, J. H. Update on drug development targeting parasite cysteine proteases. *PLoS Neglected Trop. Dis.* **2018**, *12* (8), No. e0005850.
(44) Palmer, J. T.; Rasnick, D.; Klaus, J. L.; Brömme, D. Vinyl sulfones as mechanism-based cysteine protease inhibitors. *J. Med. Chem.* **1995**, *38* (17), 3193−3196.
(45) Pereira, A. R.; Kale, A. J.; Fenley, A. T.; Byrum, T.; Debonsi, H. M.; Gilson, M. K.; Valeriote, F. A.; Moore, B. S.; Gerwick, W. H. The carmaphycins: new proteasome inhibitors exhibiting an α,β-epoxyketone warhead from a marine cyanobacterium. *ChemBioChem* **2012**, *13* (6), 810−817.
(46) Cromm, P. M.; Crews, C. M. The Proteasome in Modern Drug Discovery: Second Life of a Highly Valuable Drug Target. *ACS Cent. Sci.* **2017**, *3* (8), 830−838.
(47) Bibo-Verdugo, B.; Jiang, Z.; Caffrey, C. R.; O'Donoghue, A. J. Targeting proteasomes in infectious organisms to combat disease. *FEBS J.* **2017**, *284* (10), 1503−1517.
(48) Besse, A.; Besse, L.; Kraus, M.; Mendez-Lopez, M.; Bader, J.; Xin, B. T.; de Bruin, G.; Maurits, E.; Overkleeft, H. S.; Driessen, C. Proteasome Inhibition in Multiple Myeloma: Head-to-Head Comparison of Currently Available Proteasome Inhibitors. *Cell Chem. Biol.* **2019**, *26* (3), 340−351.e343.
(49) Liu, Y.; Patricelli, M. P.; Cravatt, B. F. Activity-based protein profiling: the serine hydrolases. *Proc. Natl. Acad. Sci. U.S.A.* **1999**, *96* (26), 14694−14699.
(50) Porta, E. O. J.; Isern, J. A.; Kalesh, K.; Steel, P. G. Discovery of Leishmania Druggable Serine Proteases by Activity-Based Probe Profiling. *Front. Pharmacol.* **2022**, *13*, No. 929493.
(51) Manoharan, A.; Jayan, J.; Rangarajan, T. M.; Bose, K.; Benny, F.; Ipe, R. S.; Kumar, S.; Kukreti, N.; Abdelgawad, M. A.; Ghoneim, M. M.; et al. "Click Chemistry": An Emerging Tool for Developing a New Class of Structural Motifs against Various Neurodegenerative Disorders. *ACS Omega* **2023**, *8* (47), 44437−44457.
(52) Li, X.; Xiong, Y. Application of "Click" Chemistry in Biomedical Hydrogels. *ACS Omega* **2022**, *7* (42), 36918−36928.
(53) Baskin, J. M.; Prescher, J. A.; Laughlin, S. T.; Agard, N. J.; Chang, P. V.; Miller, I. A.; Lo, A.; Codelli, J. A.; Bertozzi, C. R. Copper-free click chemistry for dynamic in vivo imaging. *Proc. Natl. Acad. Sci. U.S.A.* **2007**, *104* (43), 16793−16797.
(54) Leunissen, E. H. P.; Meuleners, M. H.; Verkade, J. M.; Dommerholt, J.; Hoenderop, J. G.; van Delft, F. L. Copper-free click reactions with polar bicyclononyne derivatives for modulation of cellular imaging. *ChemBioChem* **2014**, *15* (10), 1446−1451.
(55) Zanon, P. R. A.; Lewald, L.; Hacker, S. M. Isotopically Labeled Desthiobiotin Azide (isoDTB) Tags Enable Global Profiling of the Bacterial Cysteinome. *Angew. Chem., Int. Ed.* **2020**, *59* (7), 2829−2836.
(56) Leriche, G.; Chisholm, L.; Wagner, A. Cleavable linkers in chemical biology. *Bioorg. Med. Chem.* **2012**, *20* (2), 571−582.
(57) MacGregor, P.; Gonzalez-Munoz, A. L.; Jobe, F.; Taylor, M. C.; Rust, S.; Sandercock, A. M.; Macleod, O. J. S.; Van Bocxlaer, K.; Francisco, A. F.; D'Hooge, F.; et al. A single dose of antibody-drug conjugate cures a stage 1 model of African trypanosomiasis. *PLoS Neglected Trop. Dis.* **2019**, *13* (5), No. e0007373.
(58) Monti, L.; Liu, L. J.; Varricchio, C.; Lucero, B.; Alle, T.; Yang, W.; Bem-Shalom, I.; Gilson, M.; Brunden, K. R.; Brancale, A.; et al. Structure-Activity Relationships, Tolerability and Efficacy of Microtubule-Active 1,2,4-Triazolo[1,5-a]pyrimidines as Potential Candidates to Treat Human African Trypanosomiasis. *ChemMedChem* **2023**, *18* (20), No. e202300193.
(59) Francisco, K. R.; Monti, L.; Yang, W.; Park, H.; Liu, L. J.; Watkins, K.; Amarasinghe, D. K.; Nalli, M.; Polaquini, C. R.; Regasini, L. O.; et al. Structure-activity relationship of dibenzylideneacetone analogs against the neglected disease pathogen, Trypanosoma brucei. *Bioorg. Med. Chem. Lett.* **2023**, *81*, No. 129123.
(60) Mittal, N.; Davis, C.; McLean, P.; Calla, J.; Godinez-Macias, K. P.; Gardner, A.; Healey, D.; Orjuela-Sanchez, P.; Ottilie, S.; Chong, Y.; et al. Human nuclear hormone receptor activity contributes to malaria parasite liver stage development. *Cell Chem. Biol.* **2023**, *30* (5), 486−498.e487.
(61) Siqueira-Neto, J. L.; Moon, S.; Jang, J.; Yang, G.; Lee, C.; Moon, H. K.; Chatelain, E.; Genovesio, A.; Cechetto, J.; Freitas-Junior, L. H. An image-based high-content screening assay for compounds targeting intracellular Leishmania donovani amastigotes in human macrophages. *PLoS Neglected Trop. Dis.* **2012**, *6* (6), No. e1671.
(62) Shevchenko, A.; Tomas, H.; Havlis, J.; Olsen, J. V.; Mann, M. In-gel digestion for mass spectrometric characterization of proteins and proteomes. *Nat. Protoc.* **2006**, *1* (6), 2856−2860.

https://doi.org/10.1021/acsomega.4c04316
ACS Omega 2024, 9, 34829−34840